Geophys. J. Int. (2003) **152,** 20–33

Regularity and complexity of aftershock occurrence due to mechanical interactions between fault slip and fluid flow

Teruo Yamashita

Earthquake Research Institute, University of Tokyo, 1-1-1 *Yayoi, Bunkyo-ku, Tokyo* 113-0032, *Japan. E-mail: tyama@eri.u-tokyo.ac.jp*

Accepted 2002 June 11. Received 2002 April 26; in original form 2001 August 13

SUMMARY

A sequence of aftershocks is modelled assuming fluid migration in a narrow, porous fault zone formed along a vertical strike-slip fault in a semi-infinite elastic medium. The principle of the effective stress coupled to the Coulomb failure criterion introduces mechanical coupling between fault slip and pore fluid. The fluid is assumed to flow out of localized high-pressure fluid compartments in the fault zone at the instant of the main shock occurrence. We successfully simulate both regularity and complexity observed for aftershocks in a unified way. For example, we can simulate both the Omori law and the Gutenberg–Richter relation, which are the most outstanding regularity observed seismologically. A large majority of simulated aftershocks are shown to consist of repeated slips, that is, slips on fault segments that have experienced slips earlier in the aftershock sequence. Our calculations show that the emergence of the Gutenberg–Richter relation is closely related to the occurrence of these repeated slips. Complexity is also a striking feature of aftershocks. One of the examples is the occurrence of secondary aftershocks, which can also be simulated successfully if we assume several high-pressure fluid compartments formed in a fault zone or a significant change in the permeability caused by the rupture occurrence.

Key words: aftershocks, faulting, fault zone, fluid flow, permeability, seismicity.

INTRODUCTION

Aftershock occurrence is one of the most distinctive features of seismological phenomena. Almost all shallow earthquakes, regardless of size, appear to be followed by aftershocks. It has been revealed from seismological observations that there are both regularity and complexity in the occurrence of aftershocks. One of the most famil iar regularities is found for the decay rate of occurrence of aftershocks

$$n(t) \sim t^{-p}, \tag{1}$$

where p is the order of unity (Utsu 1961) and $n(t)$ is the frequency of events at time t, which is measured from the occurrence time of the main shock that triggered the aftershocks. While the relation (1) is generally referred to as the Omori law, Omori (1894) considered only the case $p = 1$. It is also well-known that aftershocks have magnitude distribution that satisfies the Gutenberg–Richter magnitude-frequency relation,

$$\log n(M) = a - bM, \tag{2}$$

where $n(M)$ is the frequency of events that occur at a given magnitude M, and a and b are constants. Utsu (1961) showed, investigating many aftershock sequences, that b is generally in the range $0.6 < b < 1.5$.

We can also observe complexity in the occurrence of aftershocks. One of the most typical examples is the occurrence of secondary aftershocks (e.g. Utsu 1970). A large-size aftershock is sometimes followed by its own aftershocks, which also satisfy the Omori law and are called secondary aftershocks. However, what should be noted is that large-size aftershocks are not always followed by the secondary aftershocks. Some researchers think that an aftershock followed by the secondary aftershocks rupture fault segments that have not slipped at the time of the main shock (e.g. Sagisaka 1927). Page (1968) considered that a large-size aftershock occurring near the outer edge of the aftershock zone tends to be followed by the secondary aftershocks.

The Omori law (1) and the Gutenberg–Richter (GR) relation (2) are exclusively mentioned as common features of aftershocks in most studies of aftershocks, and many theoretical or simulation studies have tried to explain them. However, it is also a distinctive feature of aftershocks that the aftershock area tends to expand gradually after the occurrence of the main shock (Mogi 1968, 1974; Eaton *et al.* 1970; Tajima & Kanamori 1985a,b). For example, Mogi (1968, 1974) pointed out that the aftershock area of the 1968 Tokachi–Oki earthquake showed southward expansion with an average velocity 100 km per day. However, the rate of expansion seems to be dependent on local tectonics (Tajima & Kanamori 1985a,b). Another common feature of aftershock sequences is that larger aftershocks tend to occur earlier in

an aftershock sequence (e.g. Page 1968; Eaton *et al.* 1970; Allen *et al.* 1971).

While there have been a large number of theoretical or simulation studies about the mechanism of aftershock occurrence, the aim of many researchers has been to explain the Omori law or the GR relation (e.g. Enya 1901; Burridge & Knopoff 1967; Das & Scholz 1981; Yamashita & Knopoff 1987; Dieterich 1994). However, a successful aftershock source model will at least have to explain all the features of aftershocks stated above in a unified way. A common assumption made in theoretical or simulation studies of aftershocks is the introduction of some kind of non-elasticity for the explanation of delayed ruptures in aftershock sequences. A successful source model should also be based on a physically reasonable model about the delayed ruptures.

We successfully simulate all the features of aftershocks stated above in a unified way assuming fluid migration in a fault zone as a mechanism to cause delayed ruptures. Field observations indicate fluid penetration of fault zones during slip, and a fault zone is generally regarded as a fluid conduit on the basis of petrologic studies of exhumed fault zones (e.g. McCaig 1988; Forster *et al.* 1994). Mechanical effects of fluids on earthquake faulting have been studied theoretically or experimentally in a large number of studies (e.g. Hickman *et al.* 1995). For example, Nur & Booker (1972) theoretically derived an expression for the decay of number of aftershocks on the assumption that the rate of aftershock occurrence is proportional to temporal change in pore fluid pressure. What makes a striking contrast to the study of Nur & Booker is that we in this paper simulate aftershock occurrence considering a fracture criterion for the occurrence of aftershocks. Our study here is regarded as an extension of those of Yamashita (1998, 1999), who simulated a foreshock–main shock sequence and an earthquake swarm, respectively, on the assumption of mechanical interactions between fluid flow in a fault zone and earthquake occurrence. We apply the fault zone model introduced in Yamashita (1999) with slight modifications.

It will be shown in the present paper that the Omori law and the GR relation are simulated in a unified manner in addition to other features of aftershocks. It is sometimes puzzling how such regularity as the GR relation or the Omori law emerges in apparently complex aftershock phenomena. We will show that the emergence of the GR relation is closely related to the recurrence of slip on the same location on a fault. The occurrence of secondary aftershocks can also be simulated if several high-pressure fluid sources are formed in a fault zone or a significant change is caused in the permeability by the rupture occurrence.

FLUID MIGRATION AND FAULT MODEL

The fault zone model to be assumed here is fundamentally the same as in Yamashita (1999), so that it is only briefly described here. We consider a vertical rectangular strike-slip fault S in a semi-infinite isotropic homogeneous elastic medium (Fig. 1). A narrow porous fault zone sealed from the country rock is assumed along the fault, which behaves as a fluid conduit. The remotely applied stress is assumed to be kept constant during a sequence of simulated aftershocks since the duration of aftershocks is negligibly short in comparison with the recurrence period of characteristic events on a fault.

The change in the stress p_{yx} in the country rock is assumed to be described in terms of the relative slip alone as in Yamashita (1999) since the fluid flow alone will cause negligible deformation in the country rock. Catastrophic ruptures are assumed to be instantaneous, so that a quasistatic treatment is allowed.

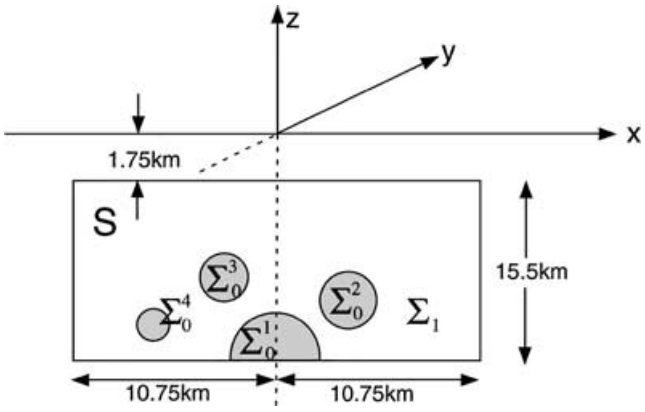

Figure 1. Elastic half-space with vertical strike-slip fault S. The fault is represented as a computational grid with a large number of segments; each segment has the size 250 m × 250 m. The plane $z = 0$ corresponds to the free surface. High-pressure fluid is initially located in the compartments $\Sigma_0^i (i = 1, \ldots, n)$; the rest of the fault, Σ_1, is under much lower fluid pressure. While we assume $n = 4$ in this illustration, most of calculations are carried out assuming $n = 1$.

According to Yamashita (1998, 1999), the governing equation for the change of the pore fluid pressure $p_f(\mathbf{x})$ in the fault zone is written as

$$\frac{\partial}{\partial x}\left(\kappa(\mathbf{x})+\frac{\partial p_f}{\partial x}\right)+\frac{\partial}{\partial z}\left(\kappa(\mathbf{x})\frac{\partial p_f}{\partial z}\right)=\eta\phi_e\beta\frac{\partial p_f}{\partial t} \tag{3}$$

by considering the continuity of fluid mass and the Darcy flow, where $\mathbf{x} = (x, z)$ is the location on the fault, η is the viscosity, ϕ_e is the elastic component of porosity, $\kappa(\mathbf{x})$ is the permeability at $\mathbf{x}$, and β is the sum of the fluid compressibility and elastic pore compressibility. We assume in the derivation of eq. (3) that the fault extent substantially exceeds the thickness of the fluid conduit, and the pore-fluid pressure p_f is regarded as the pressure averaged over the fault zone thickness. The effect of the gravity is neglected here as in Yamashita (1998, 1999). Since the consideration of relatively large plastic component of porosity has been shown to cause a rupture sequence similar to earthquake swarm (Yamashita 1999), the plastic component is assumed to be negligible in comparison with the elastic component in our calculation here.

The rupture occurrence is assumed to be dependent on the pore fluid pressure p_f through the Coulomb fracture criterion coupled to the principle of effective stress

$$\tau_s = c + m_s(\sigma_n - p_f), \tag{4}$$

where τ_s is the static shear traction at fracture, c is the cohesive strength, m_s is the coefficient of static friction and σ_n is the total normal traction on the fault. It will be reasonable to assume that the strength c drops to a lower value on a fault segment at the time of the earliest slip there in a sequence of slips because of the loss of cohesion; the value of c remains to be at the lower value for later slips there. It will be shown later in this paper that a fault segment can slip repeatedly in a sequence of simulated aftershocks. Our assumption of the strike-slip fault suggests that a rupture is initiated once the stress component p_{yx} exceeds the threshold stress τ_s; the stress p_{yx} drops suddenly to the residual level τ_f with the onset of rupture. The residual stress is also written in a form similar to (4) (Wong 1986; Yamashita & Ohnaka 1992), that is,

$$\tau_f = d + m_f(\sigma_n - p_f), \tag{5}$$

where $d(<c)$ and m_f are cohesion and coefficient of sliding friction.

We assume that the permeability increases to a higher value κ_1 from the initial value κ_0 at the instant of the earliest slip on a fault segment in a sequence of repeated slips because dynamic rupture is likely to increase the porosity and pore connectivity; the permeability is assumed to remain at the higher value κ_1 at later slips. Note that earthquake ruptures are likely to generate a large number of tensile microcracks in their vicinity (e.g. Moore & Lockner 1995; Yamasita 2000) which will increase the pore connectivity as well as the plastic component of porosity. Some formulae have been proposed for a relationship between permeability and porosity. Brace (1977) evaluated the formula

$$\kappa = \kappa_c \phi^3, \tag{6}$$

and argued that the calculated values of permeability κ compared well with measurements of a number of rock types, where ϕ is porosity and κ_c is a quantity proportional to the pore connectivity. This equation shows that the permeability is enhanced by the increases in porosity and pore connectivity. As stated before, the plastic changes in porosity were investigated in Yamashita (1999) and were shown to lead to earthquake swarms. We therefore focus on the effect of pore connectivity in this paper, and the plastic component of porosity is assumed to be negligible in comparison with the elastic component. However, quantitative effects of dynamic ruptures on κ_c are largely unknown, so that we rather arbitrarily assume the increase in the permeability κ at the instant of the earliest slip on a fault segment in a sequence of repeated slips.

As in Yamashita (1998, 1999), the rupture of an impermeable seal separating one of the high-pressure fluid compartments and the surrounding low-pressure one in a fault zone is assumed to trigger a sequence of earthquakes. Shear induced pore compaction in a sealed fault can be a mechanism for locally elevated fluid pressure (Sleep & Blanpied 1992, 1994; Byerlee 1993). We assume the spatial distribution of the pore fluid pressure at $t = -0$ in the form

$$\begin{aligned} p_f(\mathbf{x}) &= \left(p_i^{\max} - p_0\right)\sqrt{1 - (|\mathbf{x} - \mathbf{x}_i|/\xi_i)^2} + p_0 \ \mathbf{x} \in \Sigma_0^i \ (i = 1, \ldots, n) \\ &= p_0 \ \mathbf{x} \in \Sigma_1 \end{aligned} \tag{7}$$

on the fault S, where $p_i^{\max} > p_0$, and the i-th high pressure fluid compartment Σ_0^i is assumed to be located at a region to satisfy both $|\mathbf{x} - \mathbf{x}_i| < \xi_i$ and $\mathbf{x} \in S$ (Fig. 1); Σ_1 is under a lower fluid pressure p_0.

Mechanical interactions between fluid flow and rupture occurrence are caused by the abrupt changes in the permeability κ and cohesive strength c at the instant of the earliest slip at each fault segment in a sequence of slips, and through the fracture condition (4) and the boundary condition on slipped fault segments (5).

NUMERICAL CALCULATION

The fault is assumed to comprise a computational grid, in which space and time evolution of stress, relative slip and fluid pressure fields are calculated as in Yamashita (1998, 1999). All the quantities are assumed to be constant on each fault segment; each segment has the same size 250 m × 250 m. These fault segments are assumed to slip independently. The relative slip $\triangle u$, pore fluid pressure p_f, and shear stress p_{yx} are calculated at the center of each segment. The fault length and width are assumed to be 21.5 km and 15.5 km, respectively, and the top edge of the fault is at a depth of 1.75 km (Fig. 1); the rigidity and Poisson's ratio of the medium are fixed at 4.5×10^4 MPa and 0.25, respectively.

As discussed in detail by Yamashita (1998), we have no reliable information about the depth dependence of pore fluid pressure and the shear stress. We therefore make one of the simplest assumptions, that is, the shear and normal stresses and the pore fluid pressure outside of the high pressure fluid compartments are assumed to be constant over the fault at the initial state; the same assumption was made by Yamashita (1998, 1999).

The diffusion eq. (3) is solved in a finite difference scheme. Some care must, however, be taken about the calculation of the terms on the left-hand side because these terms are associated with the differentiation of discontinuous quantities; we assume abrupt increase in the permeability at the instant of the rupture occurrence. These terms are discretized following the treatment of Kummer *et al.* (1987), which was found to perform satisfactorily (Zahradnik *et al.* 1993). The stress change due to relative slips on fault segments can be calculated using an expression given by Okada (1992).

We assume as in Yamashita (1998, 1999) that the spatial distributions of p_{yx} and σ_n are constant over the fault at $t = -0$. The fluid pressure is assumed to be highest in the compartment Σ_0^1, whose rupture can therefore trigger a rupture sequence. The contribution from fault slip to the normal traction σ_n is negligible because of the narrow straight fault zone and due to the occurrence of shear slip only, so that σ_n in eqs (4) and (5) can be assumed to be constant in the calculation. Eqs (4) and (5) can therefore be rewritten as

$$\begin{aligned} \tau_s &= \alpha_s - m_s p_f, \\ \tau_f &= \alpha_f - m_f p_f, \end{aligned} \tag{8}$$

where $\alpha_s (= c - \sigma_n)$ and $\alpha_f (= d - \sigma_n)$ are parameters independent of the stress change and pore fluid pressure. The value of α_s is assumed to drop from α_s^0 to $\alpha_s^1 (> \alpha_f)$, due to a drop in cohesion c, at the instant of the earliest slip at each fault segment in a sequence of repeated slips; α_s remains at the lower value α_s^1 for later slips. We also assume $m_s = m_f = 0.7$ and the swinging back of the relative slip is prohibited as in Yamashita (1998, 1999).

EXAMPLES OF AFTERSHOCK SEQUENCES

We assume some model parameters rather arbitrarily and assume $\alpha_f = 16.5$ MPa, $p_{yx} = 10$ MPa and $p_0 = 10$ MPa at $t = -0$ in all the calculations in this paper. The strength α_s is assumed to drop from α_s^0 to α_s^1 at the instant of the earliest slip in a sequence of slips as stated in the preceding section. The initial strength α_s^0 is assumed to be distributed randomly over the fault at $t = -0$, while the relation $\alpha_s^0 - m_f p_f \leq p_{yx}$ is assumed somewhere in Σ_0^1 so that the failure of this compartment may trigger a sequence of ruptures. The strength α_s^1 is assumed to be given by a parameter $\gamma = (\alpha_s^0 - \alpha_s^1)/(\alpha_s^0 - \alpha_f)$, which is fixed in each simulation. Hence, the strength α_s drops to the level of α_f if $\gamma = 1$. If $\gamma = 0$, the cohesive strength remains unchanged; γ should therefore be in the range $0 \leq \gamma \leq 1$. The quantity α_s^0 is only the randomness in the model parameters assumed in this paper. Uniform randomness is assumed in the range from $(24 - r/2)$ MPa to $(24 + r/2)$ MPa for α_s^0 unless noted otherwise, where r is a model parameter. This suggests that the mean value of α_s^0 is fixed at 24 MPa, while its variance is changed as a model parameter. It is characteristic in our model that the tectonic shear stress p_{yx} is greater than the residual stress τ_f over the fault at

$t = -0$. Hence, the occurrence of slip is expected to release strain energy.

Now we have three fundamental model parameters, $\delta = \kappa_0/\kappa_1$, $\gamma = (\alpha_s^0 - \alpha_s^1)/(\alpha_s^0 - \alpha_f)$ and r, whose effects on the simulation results are investigated in detail in this study. Here, δ denotes the relative change in the permeability; δ should be in a range from 0 to 1 because the permeability increase from κ_0 to κ_1 with the occurrence of rupture as stated before. The parameter γ denotes a drop in cohesion, and r denotes a measure of the initial heterogeneity of the cohesive strength.

Only a single high-pressure fluid source Σ_0^1, located near the bottom of the fault, is assumed in the following calculations unless noted otherwise. The parameters describing this high-pressure fluid source are given by $\mathbf{x}_1 = (0, f_L)$, $p_1^{\max} = 20$ MPa, where $z = f_L (= -17.25$ km) is the location of the bottom edge of the fault. The value of ξ_1 is given by $17\,h (= 4.25$ km) in most examples.

Fig. 2 shows examples of simulated aftershock sequences for several values of the model parameters. The magnitude M is given by the moment magnitude, and T is nondimensional time defined as $T = \kappa_0 t / h^2 \eta \phi_e \beta$. Sudden slip occurs over a large area with the failure of the high-pressure fluid compartment, Σ_0^1, which is regarded as the main shock. The events are classified into two groups in Fig. 2. Open symbols denote a repeated slip, that is, slip on fault segments that have experienced slips earlier in each sequence; hence, no intact segment slips in an event shown by an open symbol. At least one intact fault segment slips in an event shown by a closed symbol. The slip of an intact fault segment is generally accompanied by that of the neighboring segments that have slipped earlier in the sequence as will be shown later in this paper (Figs 5a and 6a). We observe a general tendency in Fig. 2 that the size of an event is larger when the slip of an intact segment is involved, and that a large majority of the events consist of repeated slips. If no discrimination is made between the open and closed symbols, we find a general tendency for the frequency of event occurrences to decrease with time and larger size events to occur earlier in a sequence. These are commonly observed in actual aftershock sequences (e.g. Omori 1894; Eaton *et al.* 1970). It is also observed that the activity is found to be lower and the duration of activity is shorter if we assume a smaller value for γ, while qualitative features are unchanged; compare Fig 2(a) with 2(b). This occurs because it is more difficult to cause repeated slips if the cohesive strength c does not drop sufficiently. Less active sequences are also observed if the variance of the distribution of α_s^0 is smaller; compare Fig 2(a) with (c). This occurs because the population of fault segments with lower strengths is smaller in the example shown in Fig. 2(c). If we assume a smaller value for δ, the activity is found to be higher; compare Fig 2(a) with (d). This will be because the fluid tends to accumulate more easily near the rupture front when δ is small, as will be discussed in detail later in this paper. One of the distinctive features of rupture sequences observed in Fig. 2 is that secondary aftershocks follow a relatively large event only in the case $\delta = 0.01$. The mechanism of the occurrence of such secondary aftershocks will be investigated later in this paper.

As noted in Yamashita (1999), a wide variation of *in situ* estimates of the permeability is an obstacle for the quantitative simulation of interactions between earthquake rupture and fluid migration. If we assume $\eta = 2 \times 10^{-4}$ Pas, $\beta = 1 \times 10^{-8}$ Pa^{-1} and $\phi = 0.01$, then we find that $T/dT = 1 \times 10^6$ corresponds to $t = 6.94$ hours and 7.93×10^3 yr for $\kappa_0 = 10^{-11}$ m^2 and $\kappa_0 = 10^{-18}$ m^2, respectively; both are in the range of the *in situ* estimate of the permeability (Yamashita 1999). This estimate implies that the permeability κ_0 must be in a limited range for the sequences shown in Fig. 2 to simulate the duration of actual aftershocks successfully.

FREQUENCY DISTRIBUTION OF MAGNITUDES

The frequency-magnitude curves that result from the simulations are illustrated in Figs 3(a) and (b) for some examples; the effects of δ, r and ξ_1 are investigated here. The value of γ is fixed at 0.99 in these figures since the number of simulated events is too small for a statistical analysis for $\gamma < 0.9$. We observe a feature common in each curve that the frequency-magnitude distribution for the events includes a scaling region of small-size events that is similar to the GR relation, and a region of large-size events whose frequency exceeds that of the extrapolated GR relation. The b value of the GR relation for small-size events is found to be in the range from 1.0 to 1.2 in our simulations (Figs 3a and b) and is almost independent of the assumed model parameters. The b values obtained in the simulations is in accordance with seismological observations: Utsu (1961) obtained the b values in the range from 0.6 to 1.5 in the analysis of 30 aftershock sequences.

Frequency distributions with two branches, similar to the ones shown in Figs 3(a) and (b), have been reported from the analysis of earthquake catalogues. Since aftershocks generally prevail in many earthquake catalogues, such distributions will approximately represent the distributions of aftershock magnitudes. In fact, Knopoff (2001) pointed out in the analysis of an earthquake catalogue of the Southern California region that frequency distribution of aftershock magnitudes has two branches similar to the curves in Figs 3(a) and (b). However, while the crossover occurs near $M = 3.5$ in our simulations, it occurs near $M = 4.8$ in the study of Knopoff. That the frequency distribution of aftershock magnitudes has two branches implies the existence of a scale size corresponding to the crossover magnitude.

We now investigate the mechanism to cause two branches in the frequency distribution of magnitudes. The frequency distributions of magnitudes are separately illustrated, in Fig. 3(c), for repeated slips and for events that involve the slip of intact segment for the example with $r = 12.0$ and $\delta = 0.1$ shown in Fig. 3(a). It is clearly observed in Fig. 3(c) that the repeated slips obey the GR relation for all magnitudes, while no such regularity is found if the slip of intact segment is involved. The same feature is observed in our simulations even if we change the values of the model parameters. This is the reason why the frequency distribution of magnitudes tends to deviate from the GR relation at large magnitudes in Figs 3(a) and (b). Events shown with open circles have a lower threshold magnitude near $M = 3.0$ in Fig. 3(c), which is related to the assumed size of fault segment 250 m $\times$ 250 m. In fact, our simulations show that an event with $M \simeq 3$ causes slip on a single intact segment and on its neighboring segments that have experienced slips earlier. Hence, we can judge that the crossover magnitude is determined by the assumed size of fault segment, so that the emergence of the crossover magnitude near $M = 3.5$ is entirely artificial. However, seismological studies have shown that slip distribution on the fault plane of a large earthquake is highly inhomogeneous (e.g. Yoshida *et al.* 1996). Such slip maps therefore imply the existence of small-scale fault segments that can slip somewhat independently. If such fault segments actually exist on a fault, a crossover magnitude should be observed and it will depend on the frequency distribution of the sizes of fault segments. Knopoff (2001), however, attributed the crossover magnitude to the fault zone thickness having a size of

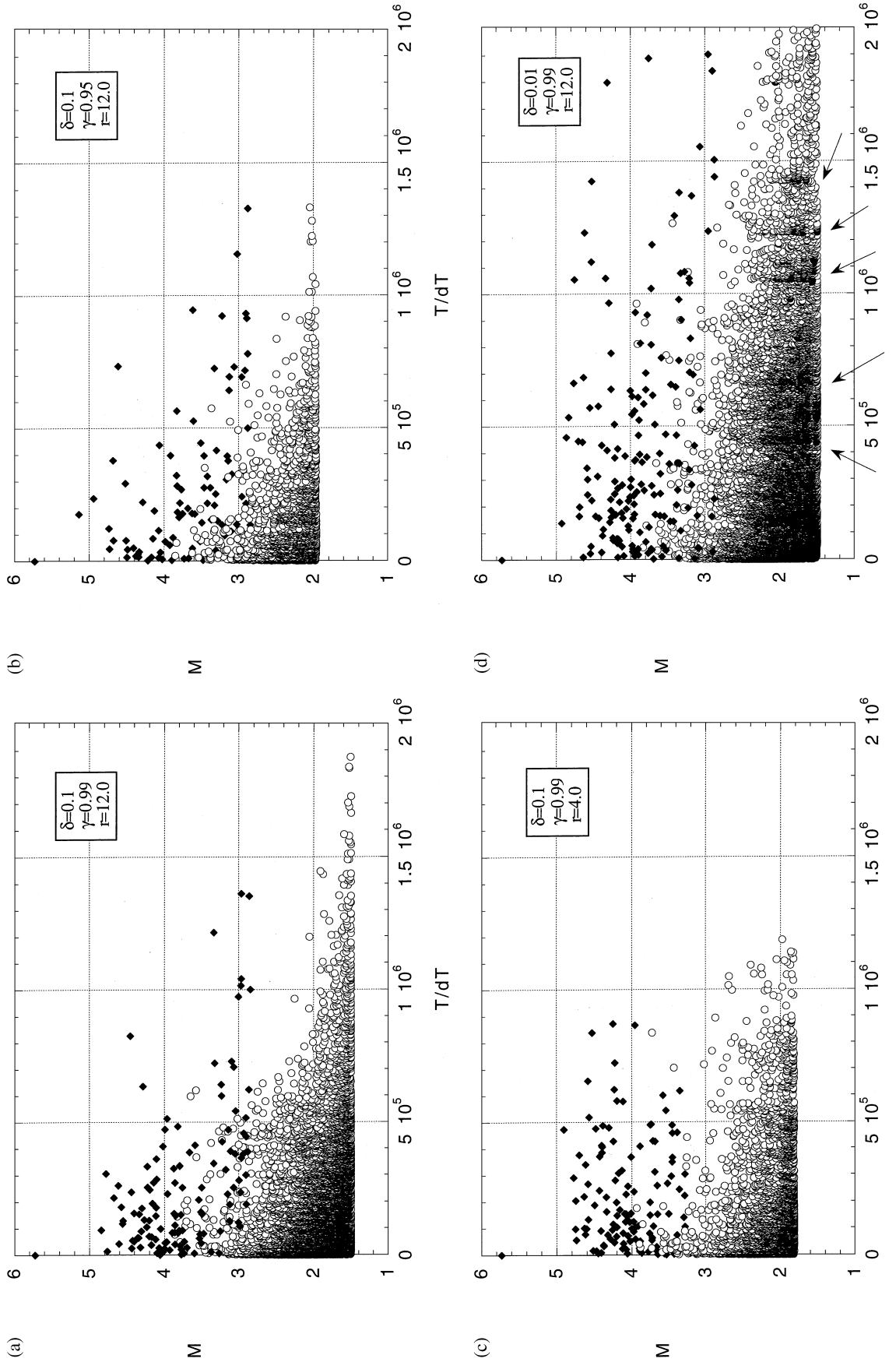

Figure 2. Dependence of temporal variation of simulated aftershock activity on the model parameters; ξ_1 is fixed at 17 h (= 4.25 km) in all the examples. The event with $M = 5.73$ occurring at $T = 0$ is the main shock in each sequence, and $dT(= 0.2 \times 10^{-3})$ is the nondimensional time increment in the numerical calculation. Open symbols denote repeated slips, whereas closed symbols denote events that rupture at least partially intact rock. We investigate the changes in behavior due to changes in γ (cohesion), r (degree of heterogeneity) and δ (permeability) in (b), (c) and (d), all with respect to the case shown in (a). Some examples of secondary aftershocks are shown by arrows in (d).

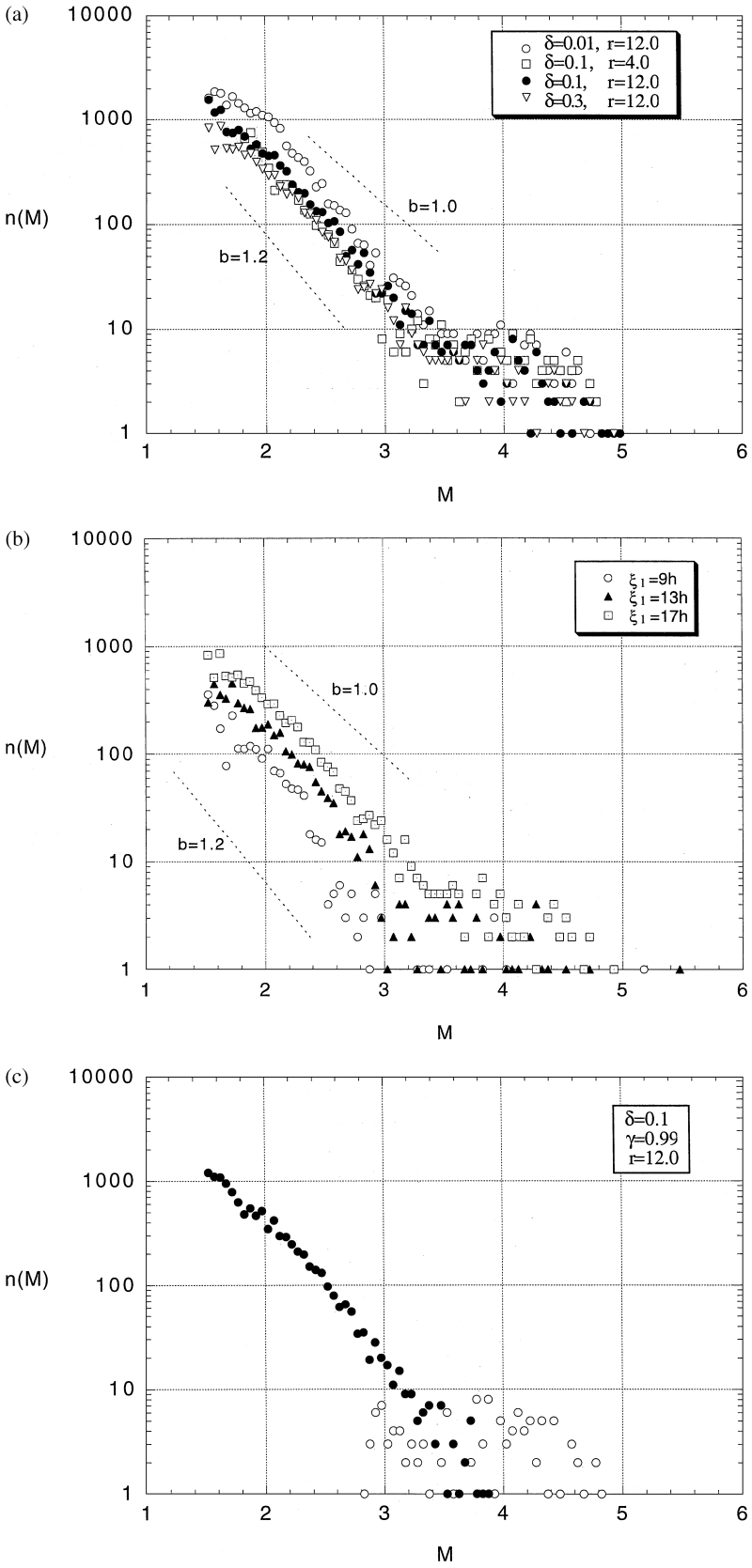

Figure 3. (a) Frequency distribution of magnitudes of simulated aftershocks; dependence on the values of δ and r is investigated. The values of γ and ξ_1 are fixed at 0.99 and 17 h(= 4.25 km) in each example. The frequency distributions are calculated from the sequences shown in Fig. 2 except the example with $\delta = 0.3$. (b) Frequency distribution of magnitudes of simulated aftershocks; dependence on the value of ξ_1 is investigated. The values of δ, r and γ are fixed at 0.3, 12.0 and 0.99, respectively, in each example. (c) Frequency distributions of magnitudes for repeated slips (closed symbol) and for events that involve a slip of, at least, one intact segment (open symbol) for the sequence of simulated aftershocks shown in Fig. 2(a).

the order of 3 km; consideration of fault zone thickness introduces another length scale.

DECAY RATE OF AFTERSHOCK OCCURRENCE

As stated in the Introduction, the decay rate of the occurrence of actual aftershocks is generally described by the Omori law, while some aftershock sequences show a deviation from the Omori law because of the occurrence of secondary aftershocks (Sagisaka 1927). The decay rate of occurrence of simulated aftershocks is illustrated in Fig. 4(a) for some examples. Only the effect of the permeability change (δ) is investigated here; r and γ are fixed at 12.0 and 0.99, respectively. It is found that the decay rate is dependent on the value of δ unlike the magnitude-frequency distributions shown in Figs 3(a) and (b). While the decay is well approximated by the Omori law for the cases $\delta = 0.1$ and 0.3, the behavior of the decay is very complicated in the case $\delta = 0.01$. This occurs because large-size events tend to generate secondary aftershocks in the case $\delta = 0.01$. Each of the secondary aftershock sequences are shown to satisfy the Omori law (Fig. 4b). We find a tendency as exemplified in Fig. 4(b) that the p value of the Omori law is smaller for an earlier sequence of secondary aftershocks. This will be because the activity is higher in an earlier time period in a sequence of simulated aftershocks.

Even if no secondary aftershocks occur, the decay rate of simulated aftershocks seems to be slightly dependent on the model parameters unlike the magnitude-frequency distribution (Fig. 4a). We now investigate how the model parameters affect the decay rate; we consider only aftershock sequences that are not accompanied by secondary sequences. Figs 4(c) and (d) show that the p value tends to be larger when δ is larger or ξ_1 is smaller, and that the p value is in the range from 0.75 to 1.2. Utsu (1961) showed that many aftershock sequences satisfy the range $0.9 < p < 1.5$ although the p value tends to vary with sequences. While the p values shown in Figs 4(c) and (d) approximately satisfy this seismological observation, the simulations suggests that the values of the model parameters should be in certain ranges to explain the seismological observation of the p value.

MECHANISMS OF OCCURRENCE OF REPEATED SLIPS AND SECONDARY AFTERSHOCKS

We show, in Figs 5 and 6, examples of the spatio-temporal variations of slip and pore-fluid pressure on the fault. Figs 5 and 6 correspond to the sequences shown in Figs 2(a) and (d), respectively, so that only the magnitude of the permeability change is different in the two figures. We assume a time period in which a relatively large-size event occurs in the illustration of these figures; this large-size event can generate secondary aftershocks in the case $\delta = 0.01$ as shown in Fig. 4(a). In Figs 5(a) and 6(a), the black area denotes the slip of intact segments, while the grey area denotes the slip of fault segments that have slipped earlier in each sequence of slips. No slip is generated on the blank area at each specified time step, while the area has already slipped in earlier events. Figs 5(a) and 6(a) clearly show that if a few intact segments slip, it is always accompanied by the slip of a large number of the neighboring segments that have experienced slips earlier. It is also found that the same segment slips repeatedly in a sequence following the occurrence of a large-size event. We now investigate how fault segments slip repeatedly in a sequence of aftershocks.

We find local changes in the fluid pressure where intact segments have slipped, which are depicted by the arrows in Figs 5(b) and 6(b). These changes denote the local fluid flow caused by an increase in the permeability where intact segments have slipped. Since the strength α_s is reduced significantly there, the fluid inflow causes slips there repeatedly. Such slips are sometimes accompanied by the slip of the neighboring segments. This is the reason why repeated slips tend to occur along the edge of rupture zone in our simulation (see grey area in Figs 5a and 6a). Precise relative relocation of small aftershocks has shown that a large majority of such events tend to concentrate along the edge of the main shock fault (e.g. Nadeau & Johnson 1998; Rubin & Gillard 2000). Our calculation suggests that such small aftershocks represent repeated slips on the main shock fault.

Both models with $\delta = 0.01$ and 0.1 are shown to generate repeated slips. However, a significant difference between the two models is that the occurrence of a large-size event suddenly enhance the activity of small-size events, identified as secondary aftershocks, only in the case $\delta = 0.01$ (compare Figs 2a and d). Since the fluid flux is far larger in the rupture area than ahead of the temporarily arrested rupture front in the case $\delta \simeq 0$, the fluids tend to accumulate near the rupture front. This will cause much larger fluid pressure gradient in the case $\delta = 0.01$ near the rupture front than in the case $\delta = 0.1$; compare Fig 5(b) with 6(b). Once intact segments rupture and the expansion of the rupture front occurs, the high-pressure fluid migrates after the extended rupture front and flows into the newly ruptured area because of the increase in the permeability there. The fluid flux is much larger near the extended rupture front in the case $\delta = 0.01$ because the fluid flux is proportional to the fluid pressure gradient according to the Darcy law. Hence, a larger number of repeated slips are expected to occur near the extended rupture front in the case $\delta = 0.01$ than in the case $\delta = 0.1$; such repeated slips are identified as secondary aftershocks in the former case.

GRADUAL EXPANSION OF AFTERSHOCK ZONE

We now investigate the temporal expansion of rupture zone on the basis of our simulation results. Fig. 7 shows the temporal change of the location of the top edge of the rupture zone; the location of the top edge is measured from the bottom of the fault. The effect of fracture strength is investigated here; we assume that the value of α_s^0 ranges from 18 MPa to 30 MPa for the example shown by circles, and 22 MPa to 34 MPa for the example shown by squares; hence, while the variance of the distribution of α_s^0 is fixed, the average value is larger in the latter case. Two aftershock sequences, shown by open and closed symbols, resulting from the same statistical distribution for α_s^0 are simulated in each case. As expected, the expansion rate is smaller when the average value of strength α_s^0 is higher. It is clearly observed that the rate of the expansion of rupture zone is larger at earlier times in all the examples. It is known that the migration of seismicity sometimes shows a similar pattern (e.g. Talwani & Acree 1985; Aoyama *et al.* 2001). Talwani & Acree (1985) and Aoyama *et al.* (2001) considered that fluid migration is responsible for the seismicity migration. Aoyama *et al.* (2001) estimated the hydraulic diffusivity by fitting the arrivals of peak fluid pressure, expected from an analysis of a diffusion equation, with the migration front of seismicity. Our study implies that the hydraulic diffusivity cannot be estimated from such an approach since the expansion of rupture zone is affected by the fracture strength as well as the hydraulic diffusivity. It should also be noted that while the expansion of rupture zone is

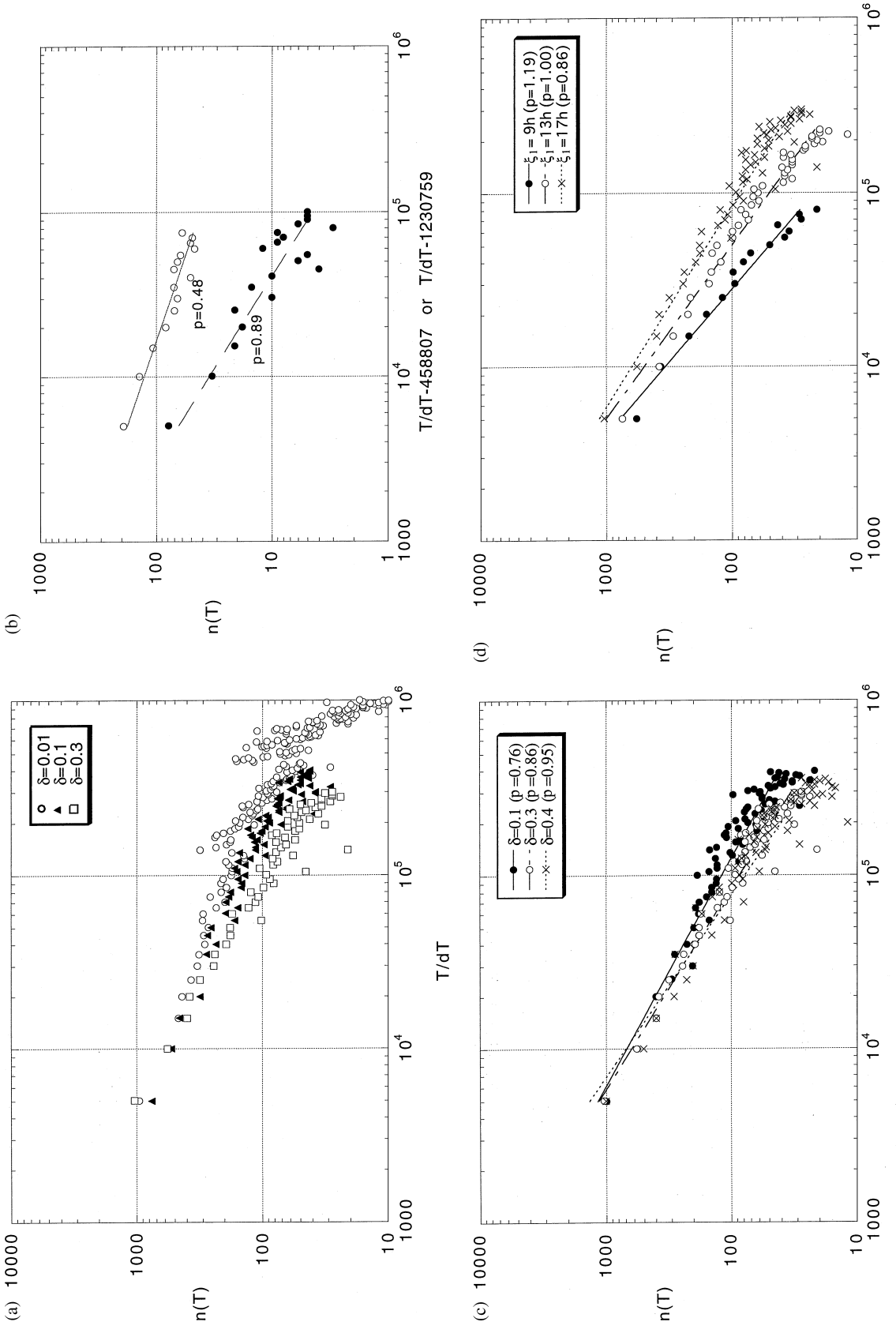

Figure 4. Temporal decay of the occurrence of simulated aftershocks. (a) Dependence of the decay on the value of δ; ξ_1, r and γ are fixed at 17 h(=4.25 km), 0.99 and 12.0, respectively. The examples with $\delta = 0.1$ and 0.01 correspond to the sequences shown in Figs 2(a) and (d), respectively. (b) Decay of the secondary aftershocks beginning at $T/dT = 458\,807$ (open symbol) and at $T/dT = 1\,230\,759$ (closed symbol) for the example shown in Fig. 2(d). The numerals denote the maximum likelihood estimate of the value of p in eq. (1) for each sequence. The abscissa denotes the nondimensional time measured from the initiation of each secondary aftershock sequence. (c) Dependence of the decay rate p of aftershocks on the value of δ; ξ_1, r and γ are fixed at 17 h(=4.25 km), 0.99 and 12.0, respectively. Each line denotes eq. (1) with a maximum likelihood estimate of the p value. (d) Dependence of the decay rate p of aftershocks on the value of ξ_1, the size of the high-pressure fluid compartment; δ, r and γ are fixed at 0.1, 0.99 and 12.0, respectively. Each line denotes eq. (1) with a maximum likelihood estimate of the p value.

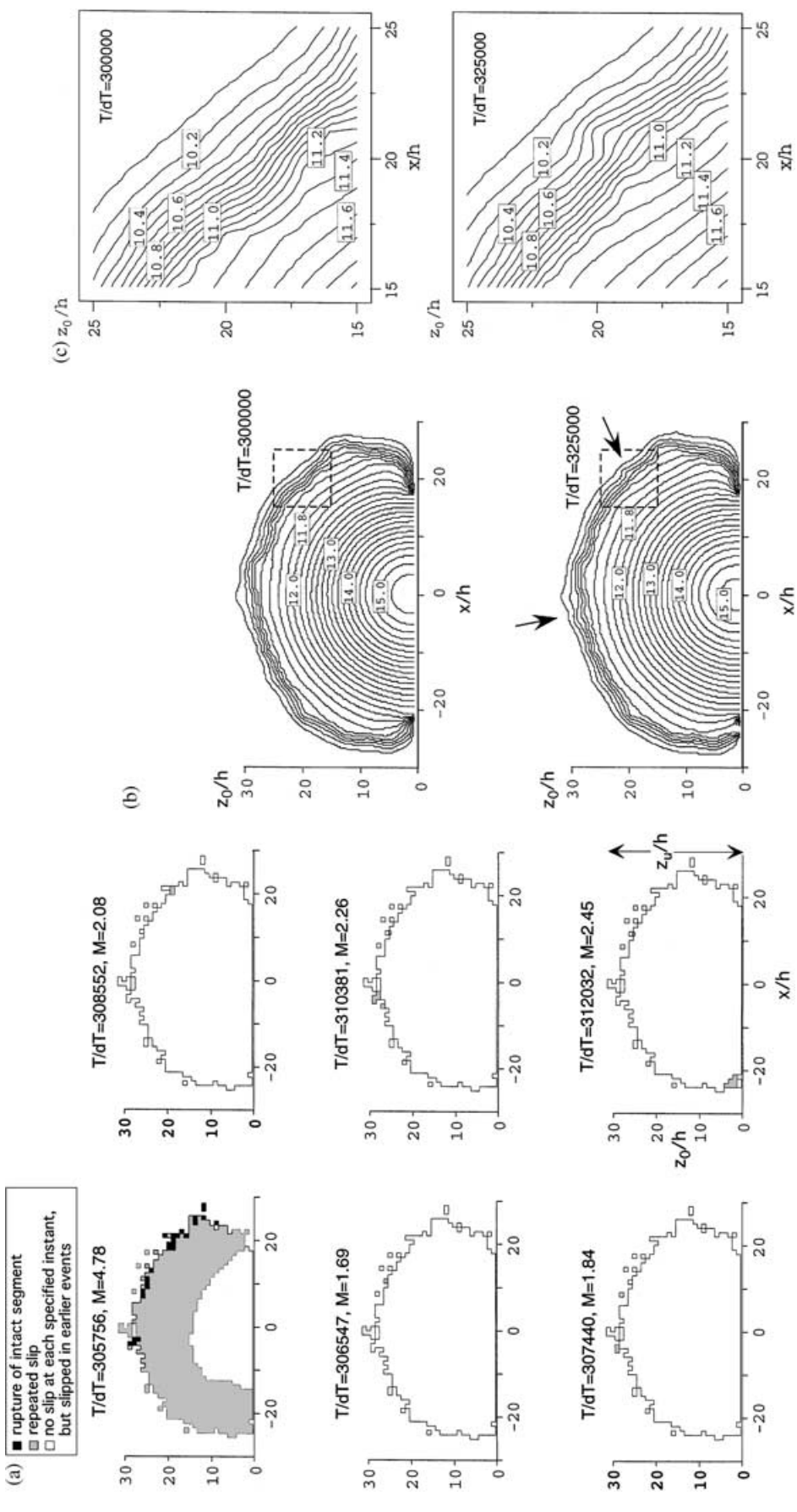

Figure 5. Spatio-temporal variations of (a) slip and (b) pore-fluid pressure for the example shown in Fig. 2(a). M and T denote the magnitude and occurrence time of each event in (a). The location of the top edge of the rupture zone measured from the bottom of the fault is denoted by z_u (see also Fig. 7). The numerals on the contours in (b) denote the fluid pressure in MPa, and z_0 is the distance from the bottom of the fault. The arrows in (b) denote local perturbations of fluid pressure due to slips of intact segments. The pore-fluid distribution in the square zones shown in (b) is magnified in (c); the fluid pressure perturbations are observed more clearly.

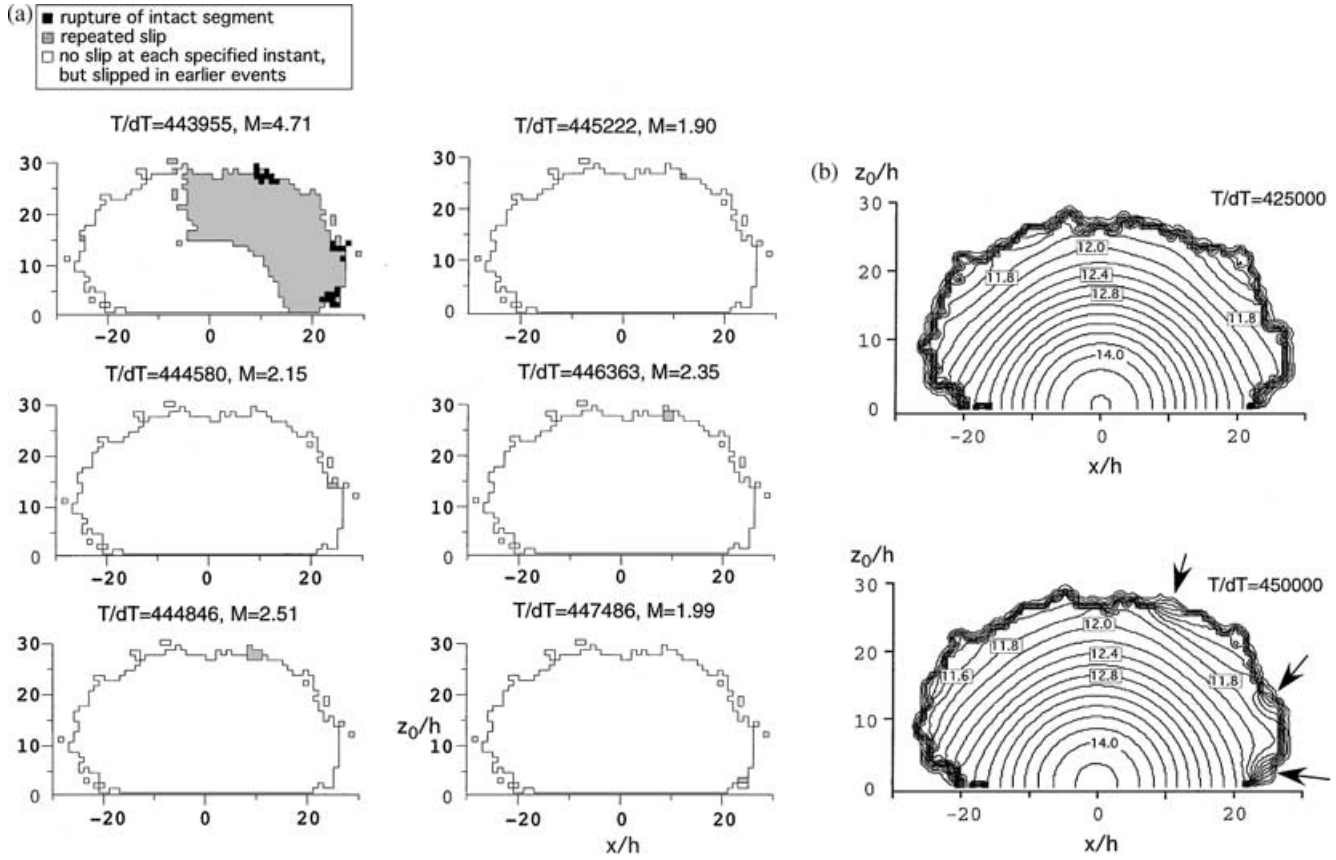

Figure 6. Spatio-temporal variation of (a) slip and (b) pore-fluid pressure for the example shown in Fig. 2(d). M and T denote the magnitude and occurrence time of each event in (a). The numerals in (b) denote the fluid pressure in MPa, and z_0 is the distance from the bottom of the fault.

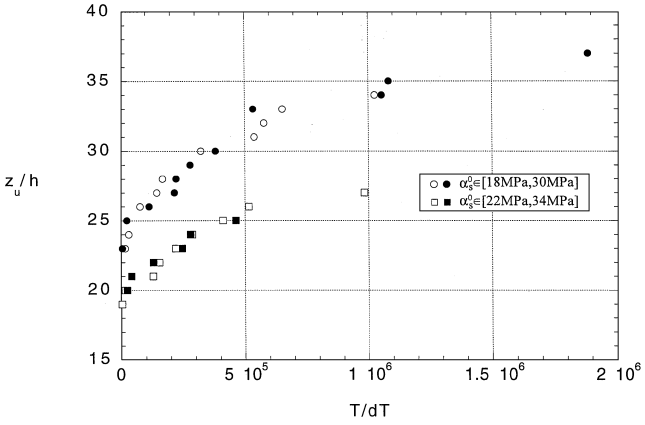

Figure 7. Temporal variation of the location of the top edge of the rupture zone for some values of the model parameters. The value of α_s^0 is assumed to range from 18 MPa to 30 MPa and 22 MPa to 34 MPa for the examples shown by circles and squares, respectively. Two aftershock sequences, shown by open and closed symbols, resulting from the same statistical distribution for α_s^0 are simulated for each case. The values of ξ_1, δ and γ are fixed at 17 h(=4.25 km), 0.1 and 0.99, respectively, in each sequence here. z_u is the location of the top edge of the rupture zone measured from the bottom of the fault (see Fig. 5a).

rather smooth in the examples shown in Fig. 7 (see also Figs 4a and 5a), it is sometimes quite irregular if we assume multiple high-pressure fluid compartments, whose effects will be investigated in the next section.

EFFECTS OF MULTIPLE HIGH-PRESSURE FLUID COMPARTMENTS

If hydraulic properties are very inhomogeneous in a fault zone, it may be more appropriate to assume several high-pressure fluid compartments there; Fitzenz & Miller (2001) actually showed the generation of such high-pressure fluid compartments in their numerical simulation. The existence of such high-pressure fluid compartments may much more complicate interactions between fluid flow and rupture occurrence. We shortly investigate the effects of multiple high-pressure fluid compartments in this section. We specifically assume four high-pressure fluid compartments Σ_0^1, Σ_0^2, Σ_0^3 and Σ_0^4 in the fault zone (see Figs 1 and 8a); their model parameters in eq. (7) are assumed to be given by $\mathbf{x}_1 = (0, f_L)$, $\mathbf{x}_2 = (0, f_L + 20h)$, $\mathbf{x}_3 = (-22\,h, f_L + 8h)$, $\mathbf{x}_4 = (19\,h, f_L + 16\,h)$, $p_1^{\max} = 20$ MPa, $p_2^{\max} = p_3^{\max} = p_4^{\max} = 15.5$ MPa, $\xi_1 = 11\,h$, $\xi_2 = \xi_3 = \xi_4 = 6\,h$, where $z = f_L(= -17.25$ km) is the location of the bottom edge of the fault and $h(= 250$ m) is the side length of each fault segment. The fluid pressure is highest in the compartment Σ_0^1, so that the failure of this compartment is expected to trigger a sequence of ruptures. We assume $\delta = 0.1$, $\gamma = 0.99$ and $r = 12$ in the calculation, which are the same as in Fig. 2(a). Hence, the difference in the assumptions made in Fig. 2(a) and here lies only in the spatial distribution of high-pressure fluid compartments.

The simulated rupture sequence is illustrated in Fig. 9(a). The main shock ruptures the whole area of the compartment Σ_0^1 and some segments in the other high pressure fluid compartments (see Fig. 8b). We find that the rupture activity is much more complex

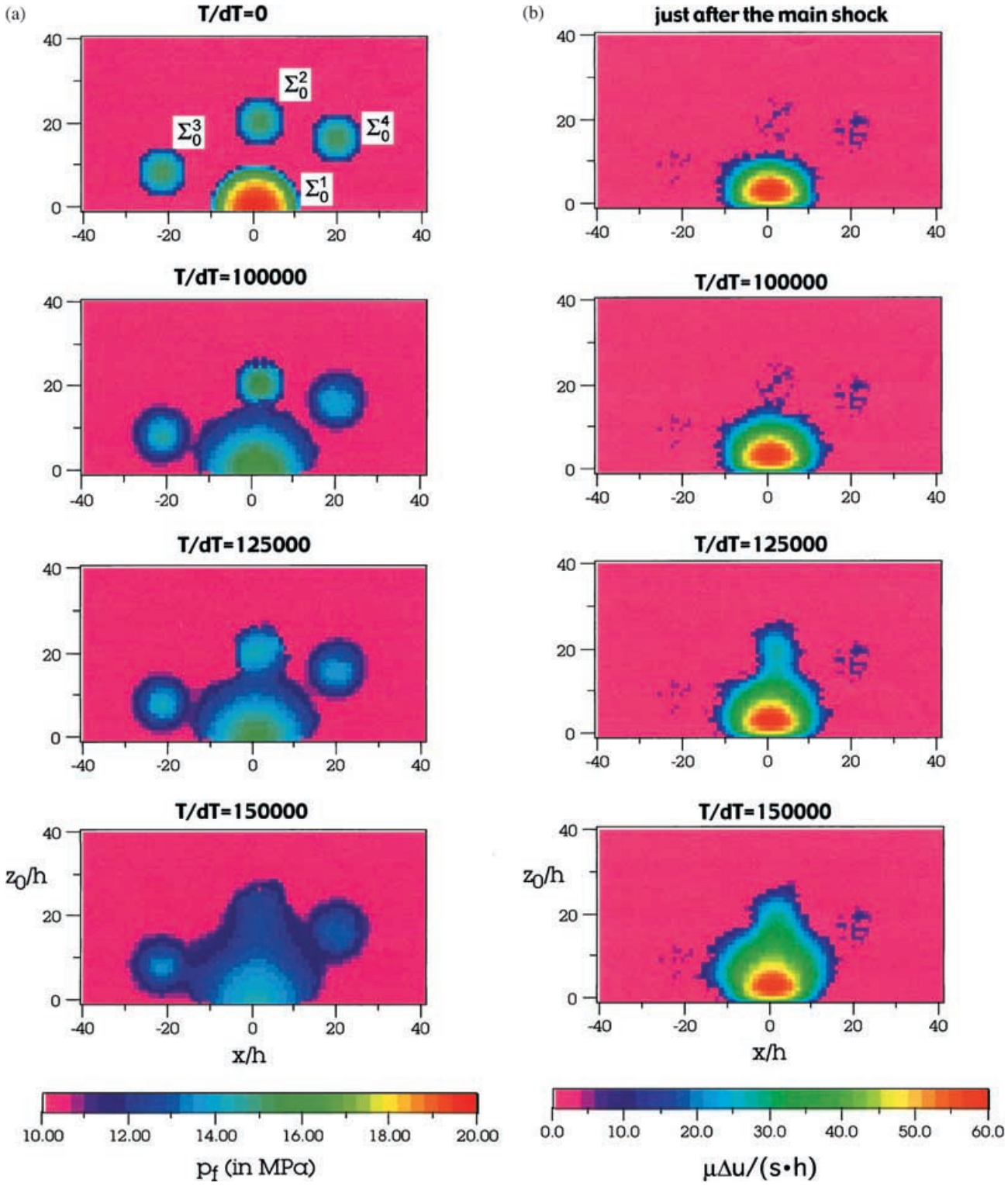

Figure 8. (a) Spatio-temporal variation of fluid pressure p_f in the case when multiple high-pressure fluid compartments are formed in the fault zone. (b) Spatio-temporal variation of slip Δu in the case when multiple high-pressure fluid compartments are formed in the fault zone; $s = 1$ MPa, $h = 250$ m and μ is the rigidity of the medium.

in Fig. 9(a) than in Fig. 2(a). The increase in the activity at $T/dT = 100\,000 \sim 130\,000$ (see also Fig. 9b) is due to the sudden coalescence of rupture zones formed at Σ_0^1 and Σ_0^2. Our calculations show that two rupture zones formed at Σ_0^1 and Σ_0^2 coalesce in the time period $T/dT = 100\,000 \sim 130\,000$ (see Fig. 8b). Fluid pressure increases at the location of coalescence due to fluid inflow as illustrated in Fig. 8(a), which will cause repeated slips there. These slips are observed as a sequence of secondary aftershocks.

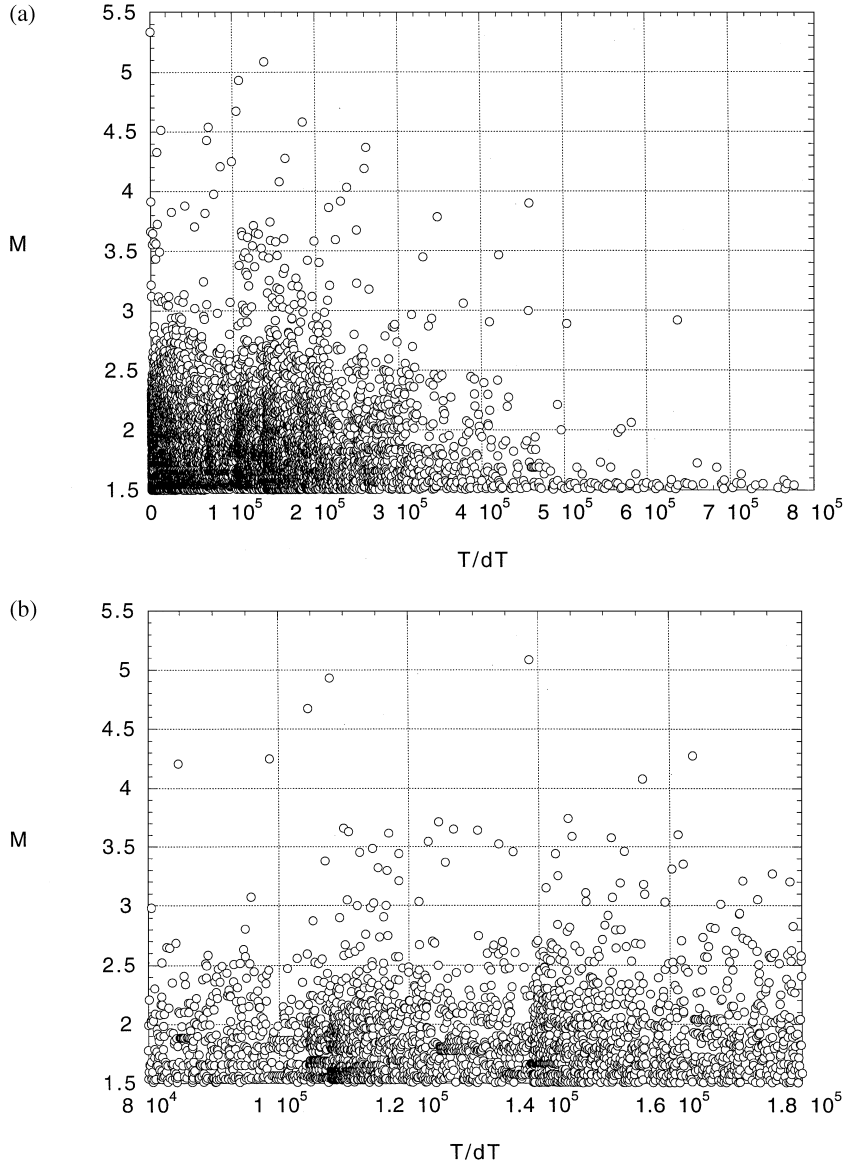

Figure 9. Temporal variation of simulated aftershock activity that corresponds to the example shown in Fig. 8. The event with $M = 5.34$ occurring at $T = 0$ denotes the main shock. The time range from $T/dT = 8 \times 10^5$ to 1.8×10^5 in (a) is magnified in (b).

DISCUSSION

We assumed in our study that the fault zone boundary is impermeable in a sequence of simulated aftershocks. However, aftershock epicenters are sometimes observed to diffuse into the country rock with time (Japan Meteorological Agency 1995). This may indicate that some parts of the fault zone boundary are fractured and become permeable because of the occurrence of the main shock. If the leakage of pore fluids occurs, the expansion of rupture zone along the fault will be smaller than simulated in the present study.

While the distribution of seismologically observed aftershock hypocenters is roughly planar, a precise determination indicates that the distribution is zonal (e.g. Hirata *et al.* 1996). This suggests that fluid flow in a zone with finite thickness must be taken into account for a more detailed and quantitative simulation. The assumption of a finite fault zone thickness introduces another characteristic scale-size in the model, which may modify the frequency distribution curves of magnitudes simulated in our study. As mentioned before, Knopoff (2001) argued that a scale size related to the fault zone thickness gives rise to two branches in the frequency distribution curve of earthquake magnitudes. Although we considered in this paper only the average flow of pore fluids in the direction parallel to the fault, we have to consider a changes in hydraulic properties across a fault zone when a finite fault zone thickness is taken into account. Field and microstructural studies of fault zones formed in rocks demonstrate that fault zones are composed, in varying amounts, of two principal components: the damage zone and the fault core (Chester *et al.* 1993; Heynekamp *et al.* 1999). Evans *et al.* (1997) found in their laboratory tests that the fault core has much lower permeabilities than the damage zone. Hence, the damage zone will act as a fluid conduit, whereas the lower permeability fault core is likely to inhibit fluid flow across the fault. This implies that fault zones have a bulk permeability anisotropy with higher permeability parallel to the fault plane and reduced permeability normal to the fault.

It is sometimes argued that the number of aftershocks is proportional to the magnitude of the main shock (e.g. Singh & Suarez 1988). We also observed such tendency in our simulation. The example shown in Fig. 2(a) has the main shock magnitude $M = 5.73$, and the number of aftershocks is 10 957. If we assume a larger fluid compartment at Σ_1 with $\xi_1 = 5.25$ km and with the same values for the other parameters as in Fig. 2(a), the main shock with larger magnitude $M = 5.92$ is simulated, and the number of simulated aftershocks is found to be 16 704. However, the number of aftershock is also dependent on such parameters as γ and δ; see Fig. 2. Dependence on local tectonics found in the relation between the main shock magnitude and the number of aftershocks (e.g. Singh & Suarez 1988) may reflect the dependence on such model parameters as γ and δ.

The unstable rupture growth is temporarily arrested in our model because of the inhomogeneities in the spatial distributions of τ_s and $\tau_0 - \tau_f$, where τ_0 is the value of p_{yx} at $t = -0$; note that the shear stress at the rupture edge is proportional to the integration of the value of $\tau_0 - \tau_f$ over the rupture surface. The fluid migration can change the distributions of τ_s and $\tau_0 - \tau_f$ (see eqs 4 and 5), so that it can trigger the regrowth of the arrested rupture. Hence, the unstable rupture growth occurs in an intermittent way in our simulations. However, the unstable rupture growth is expected to become unarrested at some time step if the value of $\tau_0 - \tau_f$ is much larger than assumed in the present study and τ_s is not much different from the value assumed here. This occurs because the shear stress at the rupture edge far exceeds the value of τ_s. If such rupture growth occurs, our aftershock model appears to be invalidated because aftershock occurrence culminates in an unstable rupture whose growth is never arrested. However, a recent analysis has shown that the spontaneous bending of the rupture plane can arrest such unstable rupture growth (Kame & Yamashita 1999a,b). While the investigation of the effect of bending of rupture plane is beyond the scope of our study, our study suggests that aftershocks can occur due to fluid migration regardless of the arresting mechanism of unstable rupture growth only if enough fluid flux exists near the temporarily arrested rupture front. The fluid flow can drive the regrowth of the temporarily arrested rupture front and a sequence of aftershocks will be observed.

The GR relation and the Omori law can also be simulated by considering the stress corrosion cracking (Yamashita & Knopoff 1987; Reuschle 1990). Although Yamashita & Knopoff (1987) did not study the occurrence of secondary aftershocks, the introduction of strong heterogeneities in fracture strengths may simulate secondary aftershocks in their aftershock models, too. However, one of the important differences is that repeated slips cannot be simulated in the models proposed by Yamashita & Knopoff (1987). We found in this paper that a large majority of simulated aftershocks consist of repeated slips, which satisfy the GR relation over all magnitudes.

CONCLUSIONS

The mechanical interactions between the rupture occurrence and fluid migration in a fault zone was shown to give rise to an aftershock sequence satisfying the GR relation and the Omori law. A majority of simulated aftershocks consist of repeated slips. We found that the emergence of the GR relation is closely related to the occurrence of repeated slips. Repeated slips occur because of the fluid flow onto fault segments that have slipped earlier in a sequence of slips. While the GR relation and the Omori law are the most distinctive regularity seismologically observed for aftershocks, we also know the existence of complexities in aftershock sequences. One of the well-known complexities is the occurrence of secondary aftershocks. We successfully simulated secondary aftershocks if we assume several high-pressure fluid compartments formed in a fault zone or a significant change in the permeability caused by the rupture occurrence.

We find a general tendency in our simulations that the frequency of aftershock occurrence decreases with time, and larger size events occur earlier in a sequence. These are commonly observed in actual aftershock sequences (e.g. Omori 1894; Eaton *et al.* 1970). Our study shows that a majority of simulated aftershocks, which are repeated slips, occur near the rupture front. Precise relative relocation of small aftershocks has also shown that a large majority of events tend to concentrate along the edge of the main shock fault. Hence, our study suggests that such small aftershocks represent repeated slips.

The aftershock zone is found to expand with time in our simulation due to gradual fluid migration. Some researchers try to estimate the hydraulic diffusivity of the crust from the observation of the expansion rate of seismicity. However, the expansion rate is also dependent on the fracture strength as clearly found in our simulation.

ACKNOWLEDGMENTS

This research was supported in part by a grant from the Ministry of Education, Science and Culture of Japan (project 12640402). I greatly appreciate helpful and constructive comments by D.Fitzenz and St.Hergarten.

REFERENCES

Allen, C.R., Engen, G.R., Hanks, T.C., Nordquist, J.M. & Thatcher, W.R., 1971. Main shock and larger aftershocks of the San Fernando earthquake, February 9 through March 1, 1971, *Prof. Pap. US Geol. Survey,* **733,** 17–20.

Aoyama, H., Takeo, M. & Ide, S., 2001. Evolution mechanism of an earthquake swarm under the Hida Mountains, Central Japan, in 1998, *J. geophys. Res.,* in press.

Brace, W.F., 1977. Permeability from resistivity and pore shape, *J. geophys. Res.,* **82,** 3343–3349.

Brace, W.F., 1980. Permeability of crystalline and argillaceous rocks, *Int. J. Rock Mech. Min. Sci & Geomech. Abstr.,* **17,** 241–251.

Burridge, R. & Knopoff, L., 1967. Model and theoretical seismicity, *Bull. seism. Soc. Am.,* **57,** 341–371.

Byerlee, W.F., 1993. Model for episodic flow of high-pressure water in fault zones before earthquakes, *Geology,* **21,** 303–306.

Chester, F.M., Evans, J.P. & Biegel, R.L., 1993. Internal structure and weakening mechanisms of the San Andreas Fault, *J. geophys. Res.,* **98,** 771–786.

Das, S. & Scholz, C.H., 1981. Theory of time-dependent rupture in the earth, *J. geophys. Res.,* **86,** 6039–6051.

Davison, C.C. & Kozak, E.T., 1988. Hydrogeological characteristics of major fracture zones in a large granite batholith of the Canadian shield, *Proc. 4th Can./Am. Conf. Hydrogeol.,* 52–60, eds Hitchon, B. & Bachu, S., National Well Water Association, Dublin, OH.

Dieterich, J.H., 1994. A constitutive law for rate of earthquake production and its application to earthquake clustering, *J. geophys. Res.,* **99,** 2601–2618.

Eaton, J.P., O'Neill, M.E. & Murdock, J.N., 1970. Aftershocks of the 1966 Parkfield-Cholame, California, earthquakes: A detailed study, *Bull. seism. Soc. Am.,* **60,** 1151–1197.

Enya, O., 1901. On aftershocks, *Rep. Imp. Earthq. Investig. Comm.,* **35,** 35–56 (in Japanese).

Evans, J.P., Forster, C.B. & Goddard, J.V., 1997. Permeability of fault-related rocks, and implications for hydraulic structure of fault zones, *J. struct. Geology,* 1393–1404.

Fitzenz, D.D. & Miller, S.A., 2001. A forward model for earthquake generation on interacting faults including tectonics, fluids, and stress transfer, *J. geophys. Res.,* **106,** 26 689–26 706.

Forster, C.B., Goddard, J.V. & Evans, J.P., 1994. Permeability structure of a thrust fault, in *The Mechanical Involvement of Fluids in Faulting,* pp. 216–223, eds Hickman, S., Sibson, R. & Bruhn, R., USGS Open File Report 94–228, US Geological Survey, Menlo Park.

Henderson, J.R. & Maillot, B., 1997. The influence of fluid flow in fault zones on patterns of seismicity: a numerical investigation, *J. geophys. Res.,* **102,** 2915–2924.

Heynekamp, M.R., Goodwin, L.B., Mozley, P.S. & Haneberg, W.C., 1999. Controls on fault-zone architecture in poorly lithified sediments, Rio Grande Rift, New Mexico: Implications for fault-zone permeability and fluid flow, in *Faults and Subsurface Fluid Flow in the Shallow Crust, Geophysical Monograph 113,* pp. 27–49 eds Haneberg, W.C., Mozley, P.S. & Goodwin, L.B., AGU, Washington DC.

Hickman, S., Sibson, R. & Bruhn, R., 1995. Introduction to special section: mechanical involvement of fluids in faulting, *J. geophys. Res.,* **100,** 12 831–12 840.

Hirata, N. & others, 1996. Urgent joint observation of aftershocks of the 1995 Hyogo-ken Nanbu Earthquake, *J. Phys. Earth,* **44,** 317–328.

Japan Meteorological Agency, 1995. The 1995 Hyogo-ken Nanbu earthquake and its aftershocks, *Rep. Coord. Comm. Earthq. Predict.,* **54,** 584–592 (in Japanese).

Kame, N. & Yamashita, T., 1999a. A new light on arresting mechanisms of dynamic earthquake faulting, *Geophys. Res. Lett.,* **26,** 1997–2000.

Kame, N. & Yamashita, T., 1999b. Simulation of spontaneous growth of dynamic crack without constraints on the crack tip, *Geophys. J. Int.,* **139,** 345–358.

Knopoff, L., 2001. The magnitude distribution of declustered earthquakes in Southern California, *Proc. Nat. Acad. Sci.,* **97,** 11 880–11 884.

Kummer, B., Behle, A. & Dorau, F., 1987. Hybrid modeling of elastic-wave propagation in two-dimensional laterally inhomogeneous media, *Geophysics,* **52,** 765–771.

McCaig, A.M., 1988. Deep fluid circulation in fault zones, *Geology,* **16,** 867–870.

Mogi, K., 1968. Development of aftershock areas of great earthquakes, *Bull. Earthq. Res. Inst.,* **46,** 175–203.

Mogi, K., 1974. Earthquakes as fractures in the earth, *Proc. 3rd. Congr. Int. Soc. Rock Mech.,* **1,** Part A, 559–568.

Moore, D.E. & Lockner, D.A., 1995. The role of microcracking in shear-fracture propagation in granite, *J. struct. Geol.,* **17,** 95–114.

Nadeau, R.M. & Johnson, L.R., 1998. Stress studies at Parkfield, VI, Moment release rates and estimates of source parameters for small repeating earthquakes, *Bull. seimol Soc. Am.,* **88,** 790–814.

Nur, A. & Booker, J.R., 1972. Aftershocks caused by pore fluid flow? *Science,* **175,** 885–887.

Okada, Y., 1992. Internal deformation due to shear and tensile faults in a half space, *Bull. seism. Soc. Am.,* **82,** 1018–1040.

Omori, F., 1894. On after-shocks, *Rep. Imp. Earthq. Inv. Com.,* **2,** 103–138 (in Japanese).

Page, R., 1968. Aftershocks and microaftershocks of the great Alaska earthquake of 1964, *Bull. seism. Soc. Am.,* **58,** 1131–1168.

Reuschle, T., 1990. Slow crack growth and aftershock sequences, *Geophys. Res. Lett.,* **17,** 1525–1528.

Rubin, A.M. & Gillard, D., 2000. Aftershock asymmetry/rupture directivity among central San Andreas fault microearthquakes, *J. geophys. Res.,* **105,** 19 095–19 109.

Sagisaka, K., 1927. Investigation of the aftershocks of the 1927 Tango earthquake, *Quart. J. Seism.,* **3,** 107–124 (in Japanese).

Singh, S.K. & Suarez, G., 1988. Regional variation in the number of aftershocks $m_b \geq 5$ of large subduction-zone earthquakes $M_w \geq 7.0$, *Bull. seism. Soc. Am.,* **78,** 230–242.

Sleep, N.H. & Blanpied, M., 1992. Creep, compaction, and the weak rheology of major faults, *Nature,* **359,** 687–692.

Sleep, N.H. & Blanpied, M., 1994. Ductile creep and compaction : a mechanism for transiently increasing fluid pressure in mostly sealed fault zones, *Pure appl. Geophys.,* **143,** 9–40.

Talwani, P. & Acree, S., 1985. Pore pressure diffusion and the mechanism of reservoir-induced seismicity, *Pure appl. Geophys.,* **122,** 947–965.

Tajima, F. & Kanamori, H., 1985a. Global survey of aftershock area expansion pattern, *Phys. Earth planet. Int.,* **40,** 77–134.

Tajima, F. & Kanamori, H., 1985b. Aftershock area expansion and mechanical heterogeneity of fault zone within subduction zones, *Geophys. Res. Lett.,* **12,** 345–348.

Utsu, T., 1961. A statistical study on the occurrence of aftershocks, *Geophys. Mag.,* **30,** 521–605.

Utsu, T., 1970. Aftershocks and earthquake statistics (II) Further investigation of aftershocks and other earthquake sequences based on a new classification of earthquake sequences, *J. Fac. Sci. Hokkaido Univ., Ser. VII,* **3,** 197–266.

Wong, T.-F., 1986. On the normal stress dependence of the shear fracture energy, in *Earthquake Source Mechanics,* pp. 1–11, eds Das, S., Boatwright, J. & Scholz, C.H., AGU, Washington, DC.

Yamashita, T., 1998. Simulation of seismicity due to fluid migration in a fault zone, *Geophys. J. Int*., **132,** 674–686.

Yamashita, T., 1999. Pore creation due to fault slip in a fluid-permeated fault zone and its effect on seismicity, *Pure appl. Geophys.,* **155,** 625–647.

Yamasita, T., 2000. Generation of microcracks by dynamic shear rupture and its effects on the rupture growth and elastic wave radiation, *Geophys. J. Int.,* **143,** 395–406.

Yamashita, T. & Knopoff, L., 1987. Models of aftershock occurrence, *Geophys. J. R. astr. Soc.,* **91,** 13–26.

Yamashita, T., T. & Ohnaka, M., 1992. Precursory surface deformation expected from a strike-slip fault model into which rheological properties of the lithosphere are incorporated, *Tectonophysics,* **211,** 179–199.

Yoshida, S., Koketsu, K., Shibazaki, B., Sagiya, T., Kato, T. & Yoshida, Y., 1996. Joint inversion of near- and far-field waveforms and geodetic data for the rupture process of the 1995 Kobe earthquake, *J. Phys. Earth,* **44,** 437–454.

Zahradnik, J., Moczo, P. & Hron, F., 1993. Testing four elastic finite-difference schemes for behavior at discontinuities, *Bull. seism. Soc. Am.,* **83,** 107–129.